Extended reduced-order surrogate models for scalar-tensor gravity in the strong field and applications to binary pulsars and gravitational waves

Minghao Guo
Peking University, Beijing 100871, China

Junjie Zhao
School of Physics and State Key Laboratory of Nuclear Physics and Technology, Peking University, Beijing 100871, China

Lijing Shao*
Kavli Institute for Astronomy and Astrophysics, Peking University, Beijing 100871, China and
Max-Planck-Institut für Radioastronomie, Auf dem Hügel 69, D-53121 Bonn, Germany
(Dated: December 14, 2020)

We investigate the scalar-tensor gravity of Damour and Esposito-Farèse (DEF) with spontaneous scalarization phenomena developed for neutron stars. We construct reduced-order surrogate model for the derived quantities coded in the pySTGROM package that speeds up calculations at two order-of-magnitude yet still keeps accuracy at $\sim 1\%$ level, compared with the previous method. We use the package to predict the relations of a NS radius, mass, inertia moment, effective scalar coupling and relevant derived quantities to its central density. The timing of binary pulsars allows us to place some of the tightest constraints on modified theories of gravity. As an application, we apply pySTGROMX to constrain the parameters of the DEF theory with well-timed binary pulsars. Our results allow for the quick evaluation of the scalar charge in scalar-tensor theory parameter space, which has applications for gravitational wave tests of scalar-tensor theories, as well as binary pulsar experiments.

I. INTRODUCTION

Albert Einstein's theory of general relativity (GR) has been tested in many cases, e.g., the Solar System[1], the timing of binary pulsars, and the gravitational-wave (GW) observation of coalescing binary black holes (BBHs) and binary neutron stars (BNSs). All of these tests have been proven to be in line with GR.

Even with the success of GR, modified gravity are still considered. Some of them are scalar-tensor gravity theories (see [2, 3] for a review). Contemporary interest in these theories has been spurred by their potential connection to inflation and dark energy, as well as possible unified theories of quantum gravity. In this paper, we focus on a class of special mono-scalar-tensor gravity, formulated by Damour and Esposito-Farèse (DEF) [4–6]. Within a certain parameter space, it significantly modifies the level where the strong equivalence principle is violated for strongly self-gravitating NSs.

The theory of scalar-tensor gravity has been extensively investigated in the weak field, mostly from experiments in the Solar System, like the Cassini detection [7]. In the parametrized post-Newtonian (PPN) framework, it is verified to a high precision $\sim 10^{-5}$ that the DEF theory is very close to GR in the weak-field regime.

In this paper, we pay particular attention to the strong-field region, where the spontaneous scalarization phenomena are significant. With the dominant radiating component being the dipolar emission at early time, a binary system emits extra energy in addition to GR. In certain binary pulsar systems, it is a powerful means to probe the strength of dipolar contribution that can be caused by the spontaneous scalarization.

Binary pulsars have played a critical role in providing key tests of general relativity (GR) and its alternatives. Binary pulsars are able to provide some of the most important gravity tests with strongly self-gravitating bodies, particularly in the quasi-stationary strong-field gravity regime.

Recently, GWs have started to compensate with binary pulsars in probing the strong-field gravity. The first GW event of coalescing BNSs, GW170817, was detected by the LIGO/Virgo Collaboration in August 2017 [8]. GW170817 provides a powerful laboratory in the highly dynamical strong field. The spacetime of BNSs is strongly curved and highly dynamical in the vicinity of NSs in the late inspiral. If the DEF theory correctly describes the gravity, GW phase evolution of BNSs is modified. So far, limited by the sensitivity of the LIGO/Virgo detectors below tens of Hz, the precision to constrain the dipolar radiation from the short duration of GW170817 is still less than binary pulsars.

In deriving constraints on the scalar-tensor gravity, the structure of NSs needs to be solved]. Thus, the equation of state (EOS) of NS matters is essential in integrating the modified Tolman-Oppenheimer-Volkoff (TOV) equations. There are still large uncertainties in the NS EOS. In this work we choose fifteen EOSs that are all consistent with the maximum mass of NSs larger that $2M_{\odot}$. Thanks to more observations being made for pulsars at radio and X-ray wavelengths, and BNSs with an increasing statistics, the uncertainty in the nuclear EOS is to be reduced in the near future.

We design and develop a method for computing derived quantities in the scalar-tensor gravity of Damour and Esposito-Farèse (DEF) with spontaneous scalarization phenomena developed for neutron stars. We construct reduced-order surrogate model for the derived quantities and integrate the model into a python package pySTGROMX that speeds up calculations at two order-of-magnitude yet still keeps accuracy, compared with the previous method. The timing of bi-

* lshao@pku.edu.cn

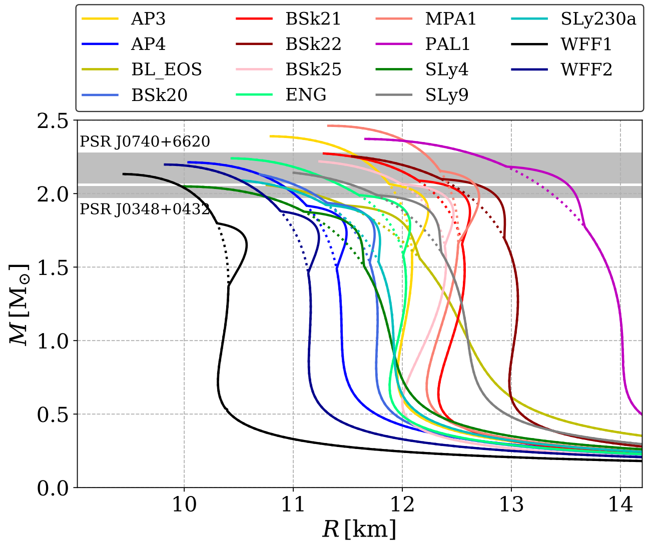

FIG. 1. Mass-radius relations of NSs for the EOSs that we adopt in this study. The mass-radius relations are derived from GR (dashed lines) and from a DEF theory with $\log_{10}|\alpha_0| = -5.0$ and $\beta_0 = -4.5$ (solid lines). The masses from PSRs J0740+6620 and J0348+0432 are overlaid in grey. The "bumps" show the deviation of the DEF theory from GR.

nary pulsars allows us to place some of the tightest constraints on modified theories of gravity. We apply pySTGROMX to constrain the parameters of the DEF theory with well-timed binary pulsars.

The rest of this paper is organized as follows. In Sec. II, we briefly review the nonperturbative spontaneous-scalarization phenomena for isolated NSs. The additional dipolar radiation and the modification of mass-radius relations for different EOSs in the scalar-tensor gravity will be discussed. Sec. III analyzes the difficulties in solving the modified TOV equations with large-scale calculations. We develop a better numerical method, and code it streamlinedly in the pySTGROMX package. We make it public for an easy use for the community. In Sec. IV, with the speedup from pySTGROMX, we stringently constrain the DEF theory by combining the dipolar radiation limits from observations of five NS-white dwarf (WD) systems and three NS-NS systems which also includes a modified mass-radius relation. Finally, the main conclusions and discussions are given in Sec. V.

II. SPONTANEOUS SCALARIZATION IN THE DEF THEORY

In this section, we study the DEF theory, which is defined by the following general action in *Einstein frame* [5, 6],

$$S = \frac{c^4}{16\pi G_\star}\int \frac{d^4x}{c}\sqrt{-g_\star}\left[R_\star - 2g_\star^{\mu\nu}\partial_\mu\varphi\partial_\nu\varphi - V(\varphi)\right] + S_m[\psi_m; A^2(\varphi)g^\star_{\mu\nu}]\,. \quad (1)$$

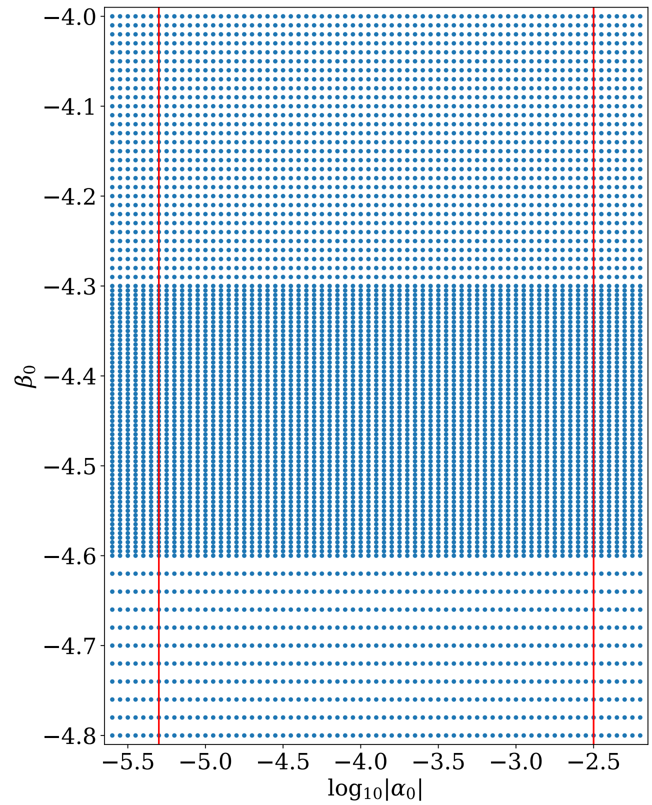

FIG. 2. An uneven grid in the parameter space $(\log_{10}|\alpha_0|, -\beta_0)$ for calculating β_A and k_A and building ROMs. We generate a set of $69 \times 101 = 6969$ parameter pairs as the training data. The region between red lines corresponds to the data we use in later calculation.

Here, $G_\star$ denotes the bare gravitational constant, $g_\star \equiv \det g^\star_{\mu\nu}$ is the determinant of Einstein metric $g^\star_{\mu\nu}$, $R_\star$ is the Ricci curvature scalar of $g^\star_{\mu\nu}$, and φ is a dynamical scalar field. In the last term of Eq. (1), ψ_m denotes matter fields collectively, and the conformal coupling factor $A(\varphi)$ describes how φ couples to ψ_m in Einstein frame. Varying the action (1) yields the field equations,

$$R^\star_{\mu\nu} = \partial_\mu\varphi\partial_\nu\varphi + \frac{8\pi G_\star}{c^4}\left(T^\star_{\mu\nu} - \frac{1}{2}T^\star g^\star_{\mu\nu}\right), \quad (2)$$

$$\Box_{g^\star}\varphi = -\frac{4\pi G_\star}{c^4}\alpha(\varphi)T_\star\,, \quad (3)$$

where $T_\star^{\mu\nu} \equiv 2c(-g_\star)^{-1/2}\delta S_m/\delta g^\star_{\mu\nu}$ denotes the matter stress-energy tensor, and $T^\star \equiv g^\star_{\mu\nu}T_\star^{\mu\nu}$ is the trace. In Eq. (3), the quantity $\alpha(\varphi)$ is defined as the logarithmic derivative of $A(\varphi)$,

$$\alpha(\varphi) \equiv \frac{\partial \ln A(\varphi)}{\partial\varphi}\,, \quad (4)$$

which indicates the coupling strength between the scalar field and matters.

In the DEF theory [6], $\ln A(\varphi)$ is designated as

$$\ln A(\varphi) = \frac{1}{2}\beta_0\varphi^2\,. \quad (5)$$

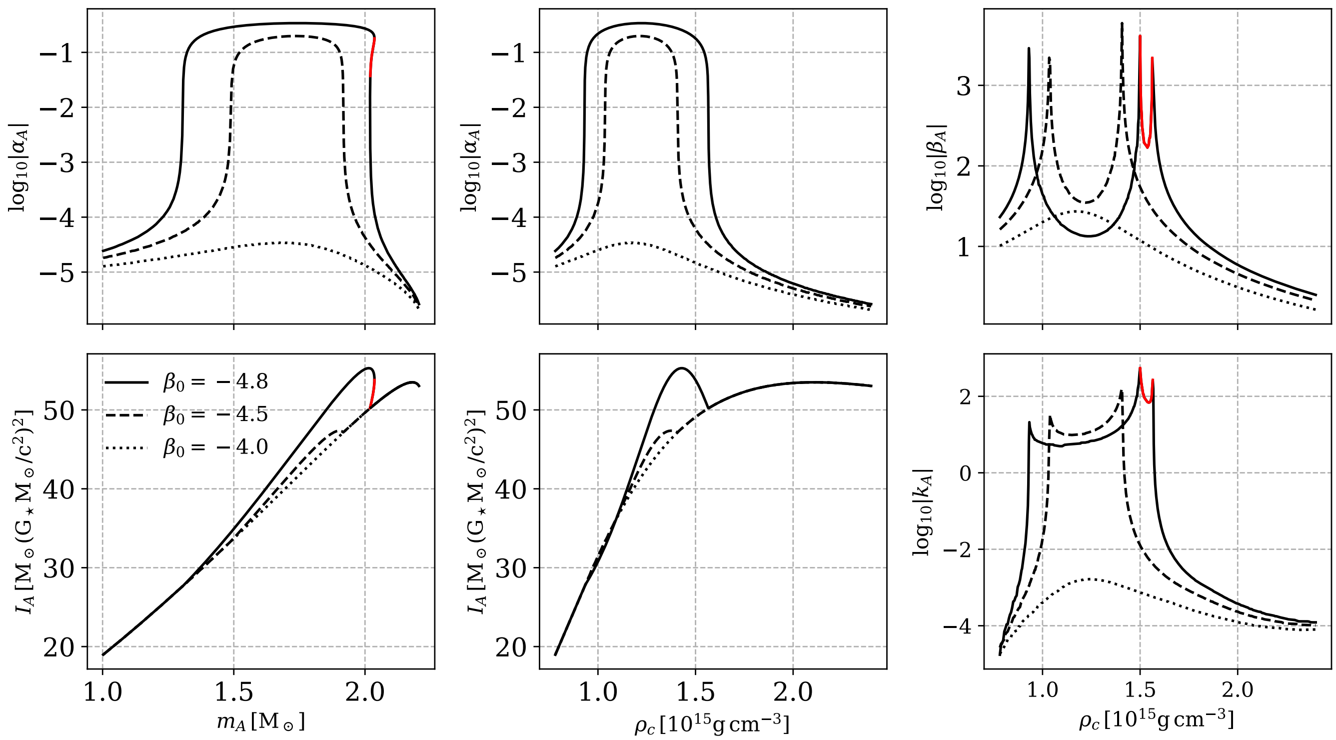

FIG. 3. Pathological phenomena occur when integrating the modified TOV equations for the EOS AP4. The calculation assumes the DEF parameters $\log_{10}|\alpha_0| = -5.3$ and $\beta_0 = -4.8$ (solid lines), -4.5 (dashed lines) and -4.0 (dotted lines). For $\log_{10}|\alpha_0| = -5.3$, the scalar field is weak for $\beta_0 = -4.0$, strong for $\beta_0 = -4.5$, and this causes the pathological phenomena for $\beta_0 = -4.8$. The red lines mark the pathological region. In this region, β_A and k_A are negative.

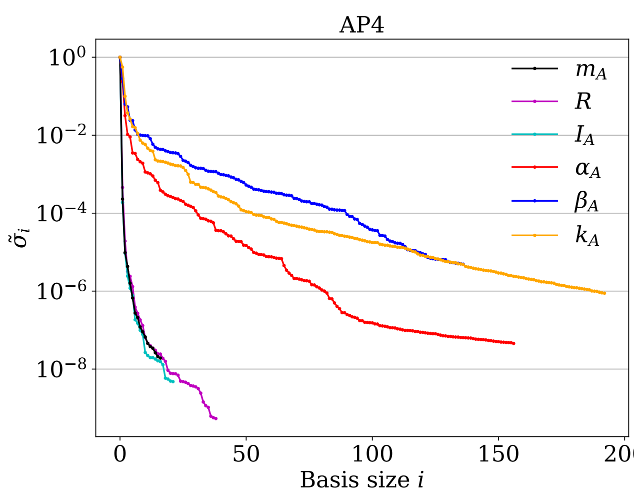

FIG. 4. Relative maximum projection error, $\tilde{\sigma}_i$, in building the ROMs for the EOS AP4. We set $\Sigma = 10^{-7}$ for m_A, R and I_A, $\Sigma = 10^{-5}$ for α_A, and $\Sigma = 10^{-4}$ for β_A and k_A.

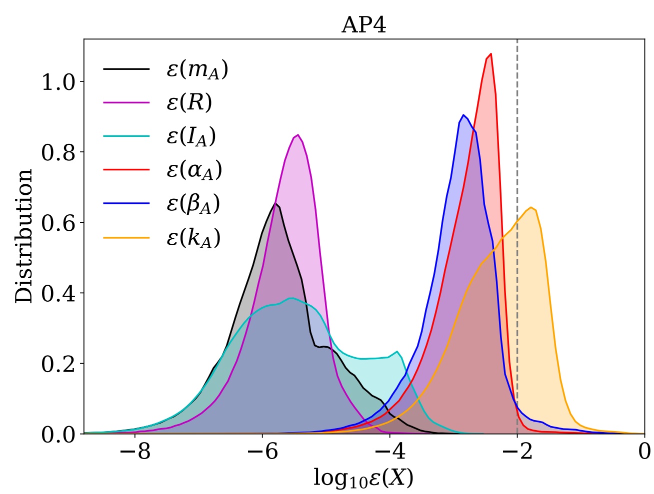

FIG. 5. Kernel density estimation (KDE) distribution of the relative error $\varepsilon(X)$, where $X \in \{m_A, R, I_A, \alpha_A, \beta_A, k_A\}$. The dashed line shows the relative tolerable error in the TOV integration ($\lesssim 1\%$).

Then $\alpha(\varphi) = \partial \ln A(\varphi)/\partial\varphi = \beta_0\varphi$. We designate $\alpha_0 \equiv \beta_0\varphi_0$, where φ_0 is the asymptotic scalar field value of φ at spatial infinity. Note that we have $\alpha_0 = \beta_0 = 0$ in GR.

For NSs, nonperturbative scalarization phenomena develop when [5, 9]

$$\beta_0 \equiv \left.\frac{\partial^2 \ln A(\varphi)}{\partial\varphi^2}\right|_{\varphi=\varphi_0} \lesssim -4\,. \tag{6}$$

Generally, a more negative β_0 means more manifest spontaneous scalarization in the strong-field regime. In such case, the *effective scalar coupling* for a NS "A" with Arnowitt–Deser–Misner (ADM) mass m_A is

$$\alpha_A \equiv \left.\frac{\partial \ln m_A(\varphi)}{\partial\varphi}\right|_{\varphi=\varphi_0}, \tag{7}$$

which measures the coupling strength between the scalar field and the NS.

Now we consider a scalarized NS in a binary pulsar system. For a NS binary system with the pulsar labeled "A" and its companion labeled "B", the quantities α_A and α_B contribute to the secular change of the orbital period decay $\dot{P}_b$ [6]. In this work we consider the dipolar and quadrupolar conribution,

$$\dot{P}_b^{\rm dipole} = -\frac{2\pi G_\star n_b}{c^3} g(e)\frac{m_A m_B}{m_A+m_B}(\alpha_A-\alpha_B)^2\,, \tag{8}$$

$$\dot{P}_b^{\rm quad} = -\frac{192\pi G_\star^{5/3} n_b^{5/3}}{5c^5} f(e)\frac{m_A m_B}{(m_A+m_B)^{1/3}}\,, \tag{9}$$

where $n_b \equiv 2\pi/P_b$, and

$$g(e) \equiv (1-e^2)^{-5/2}\left(1+\frac{e^2}{2}\right), \tag{10}$$

$$f(e) \equiv (1-e^2)^{-7/2}\left(1+\frac{73}{24}e^2+\frac{37}{94}e^4\right). \tag{11}$$

We approximate the bare gravitational constant $G_\star$ in the above equations with the Newtonian constant $G_N = G_\star(1+\alpha_0^2)$, owing to the observation from Cassini spacecraft [7] that $|\alpha_0| \ll 1$.

Similar to α_A, we define

$$\beta_A \equiv \left.\frac{\partial \alpha_A}{\partial\varphi}\right|_{\varphi=\varphi_0}, \tag{12}$$

which is the strong-field analogue of the quantity β_0. Then the theoretical prediction for the periastron advance rate is [6]

$$\dot{\omega}^{\rm th}(m_A,m_B) \equiv \frac{3n_b}{1-e^2}\left(\frac{G_{AB}(m_A+m_B)n_b}{c^3}\right)^{2/3} \times\left[\frac{1-\frac{1}{3}\alpha_A\alpha_B}{1+\alpha_A\alpha_B}-\frac{X_A\beta_B\alpha_A^2+X_B\beta_A\alpha_B^2}{6(1+\alpha_A\alpha_B)^2}\right], \tag{13}$$

where $G_{AB} \equiv G_\star(1+\alpha_A\alpha_B)$, and $X_A \equiv m_A/(m_A+m_B) \equiv 1-X_B$. Finally, consider a NS with inertia moment (in Einstein units) I_A. We denote

$$k_A \equiv \left.\frac{\partial \ln I_A}{\partial\varphi}\right|_{\varphi=\varphi_0} \tag{14}$$

as the "coupling factor" of inertia moment. The theoretical prediction of the Einstein delay parameter is [6],

$$\gamma \equiv \gamma^{\rm th}(m_A,m_B) = \frac{e}{n_b}\frac{X_B}{1+\alpha_A\alpha_B}\left(\frac{G_{AB}(m_A+m_B)n_b}{c^3}\right)^{2/3} \times[X_B(1+\alpha_A\alpha_B)+1+K_A^B]\,, \tag{15}$$

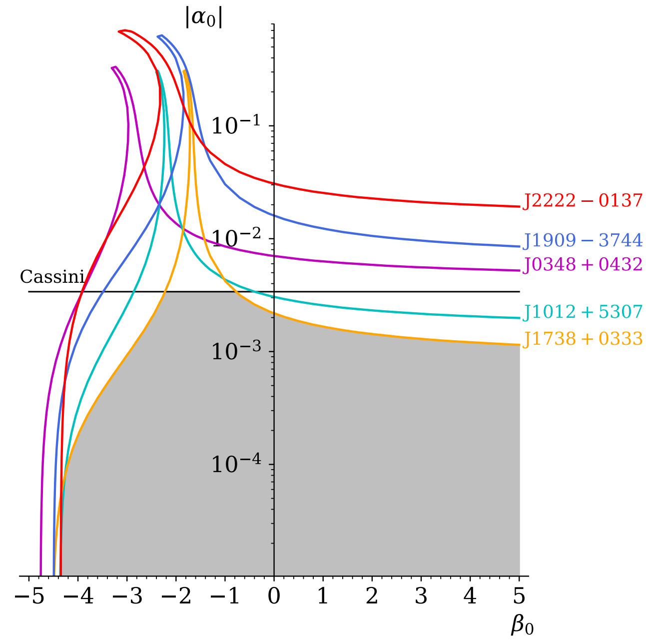

FIG. 6. Constraints on (α_0, β_0) from a variety of binary PSRs on DEF theory with the EOS AP4. Cassini stands for the measurement of a Shapiro time-delay variation in the Solar system.

where $K_A^B \equiv -\alpha_B(m_B)k_A(m_A)$ describes the contribution from the variation of I_A under the influence of the companion B. These quantities play an important role especially in double NS system, where both of the NS develop spontaneous scalarization.

III. METHODOLOGY

We here turn our attention to the calculation of the quantities in strong field. For a specific nuclear EOS of NSs, given the center mass density ρ_c and the parameters of the theory (namely, α_0, β_0), we can obtain macroscopic quantities of a NS (e.g, R, m_A, α_A and I_A), by solving the modified TOV equations with the shooting method (see Ref. [21] for details). In Fig. 1 we show mass-radius relation of NSs in the DEF theory with $\log_{10}|\alpha_0| = -5.0$ and $\beta_0 = -4.5$ for the EOSs we adopt in this study. It shows clearly that the spontaneous scalarization phenomena develop for NSs with certain masses, and lager radii are predicted in this range. However, to determine quantities β_A and k_A, we have to calculate the derivatives from Eqs. (12) and (14) for a fixed form of the conformal coupling factor $A(\varphi)$ (i.e, with a fixed β_0) and a fixed baryonic mass $\bar{m}_A$. This requires the data with different φ_0's (or equivalently, α_0's). In order to do so, we calculate the derivatives on a grid.

In practice, for each EOS, we choose the range of ρ_c so that $m_A \in (1\,{\rm M}_\odot, m_A^{\rm max})$ with the maximum NS mass $m_A^{\rm max}$ being EOS-dependent. Then we generate an uneven gird of $[\log_{10}|\alpha_0|, \beta_0] \in [-5.6,-2.2]\times[-4.8,-4.0]$, as shown in Fig. 2. The number of nodes in grid is set to $N_{\alpha_0}\times N_{\beta_0} =$

TABLE I. Binary parameters of the five NS-WD systems that we include to constrain the DEF theory (PSRs J0348+0432 [10], J1012+5307 [11–14], J1738+0333 [15], J1909-3744 [16], J2222-0137 [17]).

Name	J0348+0432	J1012+5307	J1738+0333	J1909-3744	J2222-0137
Orbital period, P_b (d)	0.102424062722(7)	0.60467271355(3)	0.3547907398724(13)	1.533449474305(5)	2.44576454(18)
Eccentricity, e	0.0000026(9)	0.0000012(3)	0.00000034(11)	0.000000115(7)	0.00038096(4)
Observed $\dot{P}_b$, $\dot{P}_b^{\rm obs}$ (fs s^{-1})	-273(45)	50(14)	-17.0(31)	-510.87(13)	200(90)
Intrinsic $\dot{P}_b$, $\dot{P}_b^{\rm int}$ (fs s^{-1})	-274(45)	-5(9)	-27.72(64)	-4.4(79)	-60(90)
Periastron advance, $\dot{\omega}$ (deg yr^{-1})	—	—	—	—	0.1001(35)
Einstein delay γ (ms)	—	—	—	—	—
Pulsar mass, m_p (M$_\odot$)	2.01(4)	—	—	1.492(14)	1.76(6)
Companion mass, m_c (M$_\odot$)	$0.1715^{+0.0045}_{-0.0030}$	0.174(7)	$0.1817^{+0.0073}_{-0.0054}$	0.209(1)	1.293(25)
Mass ratio, $q \equiv m_p/m_c$	11.70(13)	10.5(5)	8.1(2)	—	—

TABLE II. Binary parameters of the three NS-NS systems that we use to constrain the DEF theory (PSRs B1913+16 [18], J0737-3039A [19], J1757-1854 [20]).

Name	B1913+16	J0737-3039A	J1757-1854
Orbital period, P_b (d)	0.322997448918(3)	0.10225156248(5)	0.18353783587(5)
Eccentricity, e	0.6171340(4)	0.0877775(9)	0.6058142(10)
Observed $\dot{P}_b$, $\dot{P}_b^{\rm obs}$ (fs s^{-1})	-2423(1)	-1252(17)	-5300(200)
Intrinsic $\dot{P}_b$, $\dot{P}_b^{\rm int}$ (fs s^{-1})	-2398(4)	-1252(17)	-5300(240)
Periastron advance, $\dot{\omega}$ (deg yr^{-1})	4.226585(4)	16.89947(68)	10.3651(2)
Einstein delay γ (ms)	4.307(4)	0.3856(26)	3.587(12)
Pulsar mass, m_p (M$_\odot$)	1.438(1)	1.3381(7)	1.3384(9)
Companion mass, m_c (M$_\odot$)	1.390(1)	1.2489(7)	1.3946(9)
Mass ratio, $q \equiv m_p/m_c$	—	—	—

$69 \times 101 = 6969$. We calculate β_A and k_A on each node with a reasonable differential step. Finally, we use the data of $\log_{10}|\alpha_0| \in [-5.3, -2.5]$ for further calculation to avoid the inaccuracy of derivatives at boundaries. The boundary value $\alpha_0 \approx 10^{-2.5}$ is the upper limit given by the Cassini spacecraft [22], and $\beta_0 \lesssim -4.0$ corresponds to values where spontaneous scalarization happens in the DEF theory.

We have to point it out that in practice it is difficult to calculate k_A when the scalar field is weak. In this case, a change in I_A due to the weak field is comparable to the random noises during the integration in solving the modified TOV equations. The calculation of k_A is therefore not accurate. Here we propose a reasonable approximation that $k_A \sim \varphi_0^2$ when the spontaneous scalarization is not excited. Based on this assumption, we choose a large differential step and calculate $k_A = 2\varphi \partial \ln I_A / \partial \varphi^2$ to reduce the influence of numerical noises.

Due to the time-consuming computation of the TOV integration and the shooting method for large-scale calculations, such as the parameter estimation with the MCMC approach, we build ROMs for the quantities to improve the efficiency [21, 23]. In brief, to generate a ROM for a curve $h(t;\lambda)$ with parameters λ, one provides a training space of data $\mathbf{V} \equiv \{h(t;\lambda_i)\}$ on a given grid of parameters and select a certain number (denoted as m) of bases as a chosen space $\mathbf{RV} = \{e_i\}_{i=1}^m$ with the reduced basis (RB) method. In practice, given the starting RB ($i = 0$), one iteratively seeks for m orthonormal RBs by iterating the Gram-Schmidt orthogonalization algorithm with greedy selection to minimize the maximum projection error,

$$\sigma_i \equiv \max_{h \in \mathbf{V}} \left\| h(\cdot;\lambda) - \mathcal{P}_i h(\cdot;\lambda) \right\|^2, \tag{16}$$

where $\mathcal{P}$ describes the projection of $h(t;\lambda)$ onto the span of the first i RBs. The process terminates when $\sigma_{m-1} \lesssim \Sigma$, a user-specified error bound. Then every curve in the training space is well approximated by

$$h(t;\lambda) \approx \sum_{i=1}^{m} c_i(\lambda) e_i(t) \approx \sum_{i=1}^{m} \langle h(\cdot;\lambda), e_i(\cdot) \rangle e_i(t), \tag{17}$$

where $c_i(\lambda)$ is the coefficient to be used for the ROM. Finally, one performs a fit to the parameter space, $\{\lambda_i\}$, and complete the construction of ROM. More details can be found in Ref. [21] where ROMs of α_A were built.

Extending the work by Zhao *et al.* [21], we build ROMs for six quantities, R, m_A, I_A, α_A, β_A and k_A, as functions of the central mass density ρ_c, with specialized parameters $\lambda = (\alpha_0, \beta_0)$.[1] We choose the implicit parameter ρ_c as an independent variable to avoid the the multivalued relations between m_A and R, as well as α_A and I_A [21]. We show this phenomena in Fig. 3. Due to the multivalued relations, β_A

[1] In practice, we use $\ln|I_A|$, $\ln|\alpha_A|$, $\ln|\beta_A|$, and $\ln|k_0 + k_A|$—instead of β_A and k_A—for a better numerical performance, where k_0 is an EOS-dependent constant to avoid negative values of k_A in the weak field. Generally we have $k_0 \lesssim 0.2$.

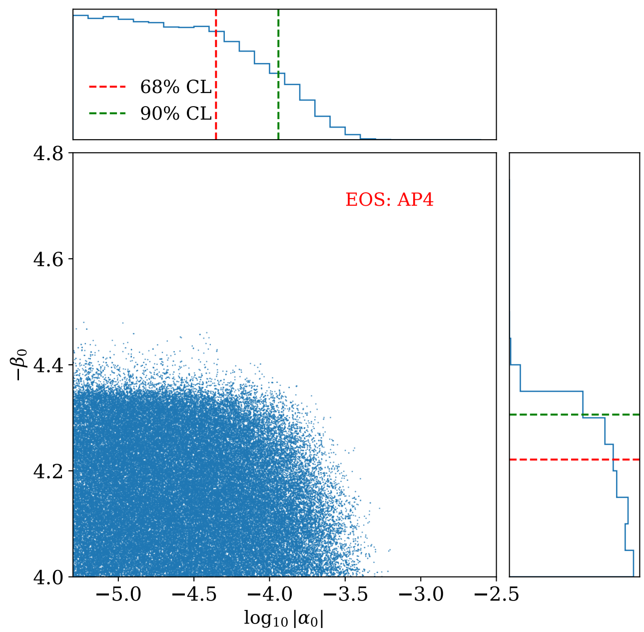

FIG. 7. The marginalized 2-dimensional distribution in the parameter space of $(\log_{10}|\alpha_0|, -\beta_0)$ from MCMC runs on the eight pulsars listed in Tables I and II for the EOS AP4. The marginalized 1-d distributions and the extraction of upper limits are illustrated in upper and right panels.

and k_A are negative when the α_A-m_A and I_A-m_A curve are bent backwards.

In balancing the computation cost and the accuracy of ROMs, we set the error bound $\Sigma = 10^{-7}$ for m_A, R and I_A, $\Sigma = 10^{-5}$ for α_A, and $\Sigma = 10^{-4}$ for β_A and k_A. The relative projection error $\tilde{\sigma_i} \equiv \sigma_i/\sigma_0$ as a function of the basis size is shown in Fig. 4. To achieve the desired projection error, the basis size is $\sim$ 20-40 for m_A, R and I_A, but $\sim$ 150-200 for α_A, β_A and k_A. This is due to the fact that there are more features in the latter set of parameters. Considering the error involved in the shooting method and the calculation of derivatives, which is $\sim 1\%$, the precision loss in ROM building is negligible.

To assess the accuracy of the ROMs, we define

$$\varepsilon(X) = \left|\frac{X_{\rm ROM} - X_{\rm mTOV}}{X_{\rm ROM} + X_{\rm mTOV}}\right|, \tag{18}$$

where $X \in \{m_A, R, I_A, \alpha_A, \beta_A, k_A\}$, to indicate the fractional accuracy of the ROMs. In Eq. (18), we denote $X_{\rm ROM}$ as the prediction of ROM, and $X_{\rm mTOV}$ as the value from the shooting algorithm and derivatives on the grid. To calculate the derivatives, we have to compute the data in a grid. Thus, instead of randomly generating parameters, we choose another grid as the test space which is shifted from the training space for α_0, β_0 and ρ_c, and calculate the quantities in the same way. The test space has sparser distribution of β_0. Note that in this method we include all errors for our ROMs, including the *interpolating* errors.

The distributions of $\varepsilon(X)$ are shown in Fig. 5. The relative errors of m_A, R and I_A are $\lesssim 10^{-5}$. On the contrary, relative errors of α_A, β_A and k_A is mostly smaller than 1%. Although this error is larger than those of R and m_A, in most cases, the error is still small enough to be neglected compared with the error from the shooting method and the calculation of derivatives. For k_A, due to the additional error from the method in calculating the derivatives, a small fraction of prediction have the error in the range $\sim 1-10\%$. This fraction generally have $k_A \ll 1$, thus has little influence.

IV. CONSTRAINTS FROM BINARY PULSARS

In this section, we apply our ROMs to constrain the parameters of DEF theory, and discuss the improvement in deriving NS properties. We combine observational results from multiple pulsar systems employing Markov chain Monte Carlo (MCMC) simulations. The efficiency is much higher than previous calculation.

A. Set up

In Table I, we show five well-timing NS-WD binary pulsars, whose mass is measured independently, in testing spontaneous scalarization: PSRs J0348+0432 [10], J1012+5307 [11–14], J1738+0333 [15], J1909-3744 [16], J2222-0137 [17]. Thus we get a satisfying results. The WD companion is a weakly self-gravitating object, leading to a tiny effective scalar coupling $\alpha_c \approx \alpha_0$. This leads to a large dipole contribution, $\propto (\alpha_A - \alpha_0)^2$, to the orbital period decay.

In Table II, we show three double NSs, PSRs B1913+16 [18], J0737-3039A [19], J1757-1854 [20]. The pulsar parameters and orbit parameters are measured by the TOA of pulses, including Keplerian and post-Keplerian parameters. Some parameters, such as the time derivative of the orbital period, $\dot{P}_b$, Periastron advance $\dot{\omega}$, Einstein delay γ are functions of the masses, and thus can be utilized to constrain the free parameters of DEF theory, α_0 and β_0.

In this study, we adopt fifteen EOSs, AP3, AP4, BL_EOS, BSk20, BSk21, BSk22, BSk25, ENG, MPA1, PAL1, SLy4, SLy9, SLy230a, WFF1, WFF2, as shown in Fig. 1. They are all consistent with the observe $2M_\odot$ maximum mass limit of NS. In addition, we adopt more EOS with radius around $\sim$ 11-13 km, owing to recent discovery about radius of NS.

It is worth noting that a completely new era for testing highly dynamical strong field with NSs has began with GW170817, thus these parameters can be used in the future detection.

First, we estimate the constraint on the DEF parameters α_0 and β_0 by saturating the bounds on individual post-Keplerian parameters. However, we need to assume a particular EOS for these constraints. From the measurements of $\dot{P}_b$, we constrain α_A and α_B by evaluating Eqs. 8 and 9. Then we further constrain $(|\alpha_0|, \beta_0)$ in region $[-5.0, 0] \times [-5.0, 5.0]$. By determining if the predicted value $\dot{P}_b^{\rm th}$ lie within the $1-\sigma$ range of $\dot{P}_b$, i.e., $\dot{P}_b \pm \delta\dot{P}_b$, we can obtain the limits on the parameter space.

In 6, we show the constraints on α_0 and β_0 for binary pulsars, assuming a EOS of AP4. Note that these constraints

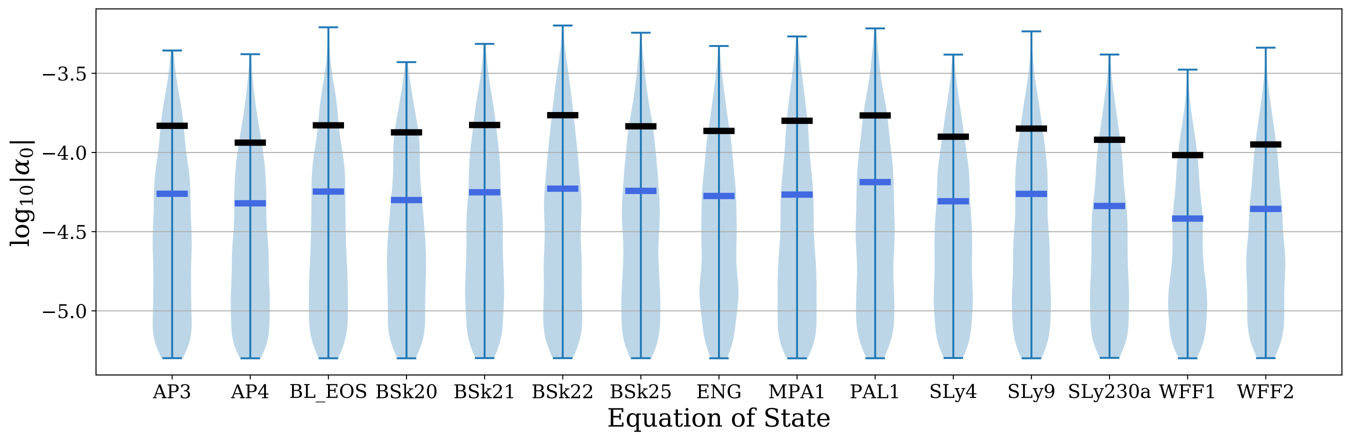

FIG. 8. The marginalized distribution in the parameter space of ($\log_{10}|\alpha_0|$) in PSRs for 15 EOSs in our studies. The 90% and 68% CL upper bounds are shown by the black and blue bars. Notice that the limit on $|\alpha_0|$ is affected by our priors (see text).

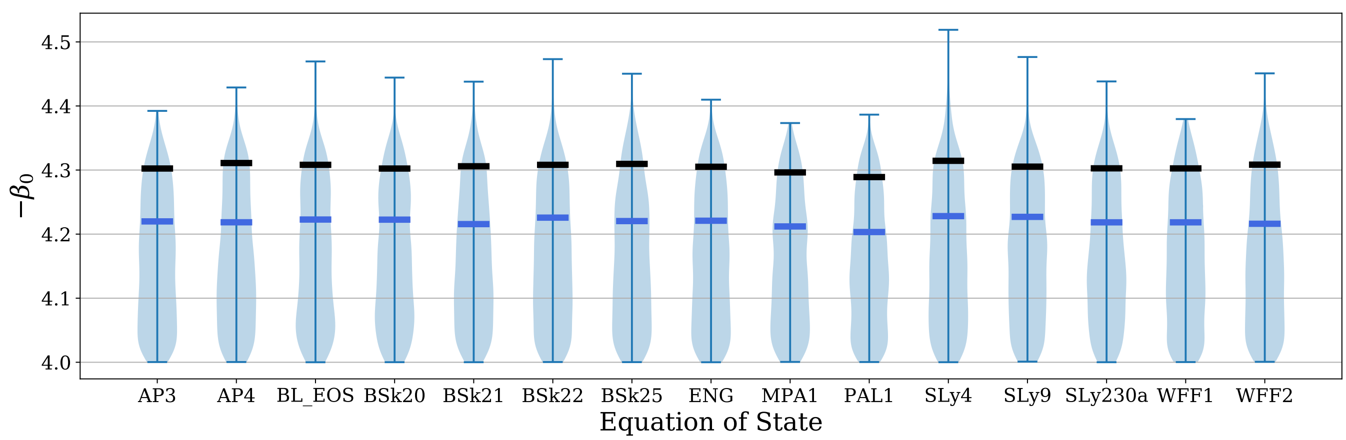

FIG. 9. Same as Fig. 8, but for the parameter $-\beta_0$.

are dependent on the specific EOS. The results are similar to previous results in [15, 24]. This diagrammatically illustrates the constraints from the timing parameters on the DEF theory. However, to determine the constraint in the strong field ($\beta_0 < -4.0$) in more details, we need more accurate method.

B. The Bayesian inference framework

We here explore constraints on the DEF theory with the well-timed binary pulsars through MCMC simulations.

In the Bayesian inference, given hypothesis $\mathcal{H}$, data $\mathcal{D}$, and priors, the posterior distribution of (α_0, β_0) can be inferred by

$$P(\alpha_0, \beta_0|\mathcal{D}, \mathcal{H}, \mathcal{I}) = \int \frac{P(\mathcal{D}|\alpha_0, \beta_0, \Xi, \mathcal{H}, \mathcal{I}) P(\alpha_0, \beta_0|, \Xi|\mathcal{H}, \mathcal{I})}{P(\mathcal{D}|\mathcal{H}, \mathcal{I})} \mathrm{d}\Xi\,, \tag{19}$$

where $\mathcal{I}$ is all the extra relevant information.

For binary pulsars, the general log-likelihood function is

$$\ln \mathcal{L}_{\rm PSR} = -\frac{1}{2}\sum_{i=1}^{N_{\rm PSR}}\left[\left(\frac{\dot{P}_b - \dot{P}_b^{\rm int}}{\sigma_{\dot{P}_b^{\rm int}}}\right) + \left(\frac{\dot{\omega} - \dot{\omega}^{\rm obs}}{\sigma_{\dot{\omega}^{\rm obs}}}\right) + \left(\frac{\gamma - \gamma^{\rm obs}}{\sigma_{\gamma^{\rm obs}}}\right) + \left(\frac{m_p - m_p^{\rm obs}}{\sigma_{m_p^{\rm obs}}}\right) + \left(\frac{m_c - m_c^{\rm obs}}{\sigma_{m_c^{\rm obs}}}\right)\right] \tag{20}$$

for $N_{\rm PSR}$ bianry pulsar systems. The likelihood function includes all contributions. However, not each pulsar's measurement of $\dot{\omega}$, γ, m_p and m_c are independent. Thus, only for some pulsars, the contributions of $\dot{\omega}$, γ are counted.

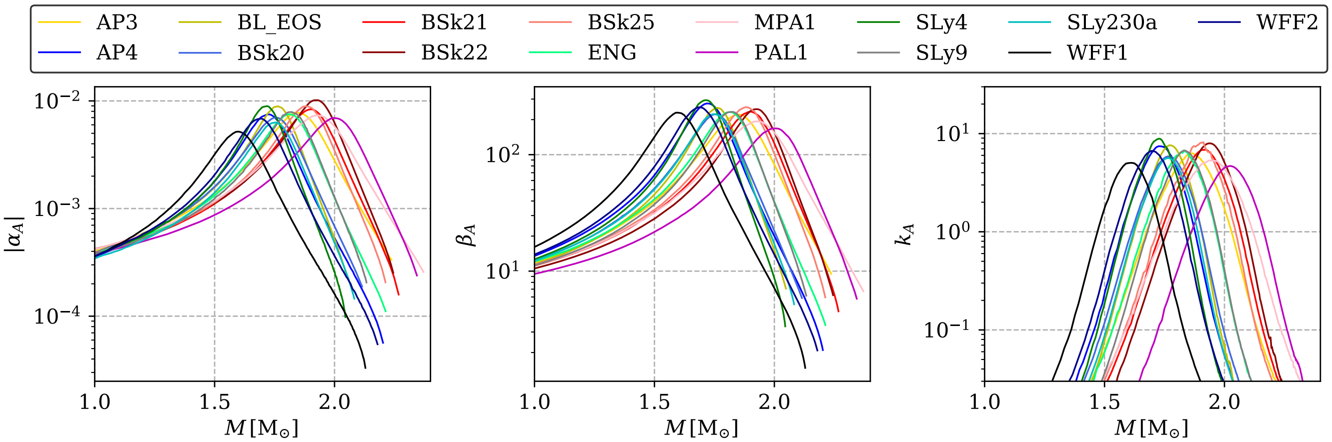

FIG. 10. The 90% CL upper bounds on the NS effective scalar coupling, α_A, β_A and k_A.

In addition to the five NS-WD bianry pulsars, that have been investigated very well in [21], we combine three extra double NS system, which utilize the information from $\dot{\omega}$ and γ. We include the contribution from γ in J0737-3039A. For any WD companions, the charges reduced to $\alpha_B = \alpha_0$ and $\beta_B = \beta_0$.

For the full calculation, we note that, for some parameters, like the orbital period P_b and the orbital eccentricity, e, we adopt their central value since they are determined very well.

For our studies, we carefully choose the priors of (α_0, β_0) so as to cover the the region where the spontaneous scalarization develops. We assume a uniform distribution of ($\log_{10}|\alpha_0|$, β_0) in the region of our ROMs. Then the parameters can be constrained by evaluating the log-likelihood function.

For the MCMC runs, we use a uniform prior on the region of our ROMs, i.e., $\alpha_0 \in [-5.6, -2.2]$, $\beta_0 \in [-4.8, -4.0]$. During the whole process, we restrict the parameters in this region of interest. Now, we employ MCMC thechnique to get the posteriors from the priors on (α_0,β_0) and the log-likelihood function. The initial values of central matter densities, ρ_c, are needed in the Jordan frame. They are fed to our ROMs to derive the NS properties. Initially they will be sampled around their GR values, but they are allowed to explore a sufficiently large range in the MCMC process. We use 24 walkers and 100000 steps for each MCMC simulation.

We perform Gelman-Rubin test for convergence and our samples have passed the test, thus our limits on α_0 and β_0 are reliable.

C. Constraints from binary pulsars

In Fig. 7, we show the marginalized 2-d posterior distribution in the parameter space of ($\log_{10}|\alpha_0|, -\beta_0$) and 1-d confidence level (CL). The results are similar to previous constraints. Here we note that in the future, with the further development of pulsar timing, $\dot{\omega}$ and γ can provide better constraints in modified gravit theories. Here we only provide a test that proves the ability of our method to constrain these parameters.

In Figs. 8 and 9, we show the distribution of $\log_{10}|\alpha_0|$ and $-\beta_0$ for all the fifteen EOSs, and their 68% and 90% CL upper bounds. These results are similar. The 90% CL upper bounds of α_0 is roughly 10^{-4}. The 90% CL upper bounds of $-\beta_0$ is roughly 4.3, where spontaneous scalarization phenomena develop. Here we nothe that the constraints on α_0 is highly influenced by the priors. But the *relative* strength of these tests does not change. A more stiff EOS would generally lead to more tight constraints.

In Fig. 10, the 90% CL upper bounds on the NS shows that the "scalarization window" [24] is still open, though slightly limited. However, the peaks of β_A and k_A shown in Fig. 3 are strongly excluded. Therefore a large deviation from GR is not expected.

In a short summary, the constraints on $|\alpha_0|$ improve with the precision of the observations. But, for β_0, not only the precision of the observations, but also the choice of the EOS can influence the limit. Different EOSs allow NSs to scalarize at different NS masses. We can use the observations, binary pulsars and BNSs, to constrain the DEF theory with different EOSs, if suitable systems are observed.

V. CONCLUSION

In this paper, we investigated the scalar-tensor gravity theory proposed by Damour and Esposito-Farèse (DEF) that predicts large deviations from General Relativity for neutron stars through spontaneous scalarization phenomena. we constructed reduced-order surrogate model for the derived quantities $m_A, R, I_A, \alpha_A, \beta_A, k_A$ in this theory, coded in a python package pySTGROMX that speeds up calculations at two orders of magnitude yet still keeps accuracy, compared with the previous algorithms. The code is made public for the community use. As an application, we utilized pySTGROMX to explore constraints on the DEF theory with latest well-timed binary pulsars and gravitational waves through MCMC simulations. We show that the "scalarization window" is still open.

Furthermore, the next-generation ground-based GW detectors are expected to observe many more systems in the future, and they can be used to study alternative gravity theories in a more precise way. Our ROMs are built to meet the requirements of new observations to constrain the DEF theory in an efficient yet accurate way. Our results allow for the quick evaluation of the scalar charge in scalar-tensor theory parameter space, which has applications for gravitational wave tests of scalar-tensor theories, as well as binary pulsar experiments.

[1] C. M. Will, Living Reviews in Relativity **17**, 4 (2014), arXiv:1403.7377 [gr-qc].

[2] C. M. Will, *Theory and Experiment in Gravitational Physics*, 2nd ed. (Cambridge University Press, 2018).

[3] Y. Fujii and K.-i. Maeda, *The Scalar-Tensor Theory of Gravitation*, Cambridge Monographs on Mathematical Physics (Cambridge University Press, 2003).

[4] T. Damour and G. Esposito-Farese, Classical and Quantum Gravity **9**, 2093 (1992).

[5] T. Damour and G. Esposito-Farèse, Phys. Rev. Lett. **70**, 2220 (1993).

[6] T. Damour and G. Esposito-Farèse, Phys. Rev. D **54**, 1474 (1996).

[7] B. Bertotti, L. Iess, and P. Tortora, Nature (London) **425**, 374 (2003).

[8] B. P. Abbott, R. Abbott, T. D. Abbott, F. Acernese, K. Ackley, C. Adams, T. Adams, P. Addesso, R. X. Adhikari, V. B. Adya, and et al., Phys. Rev. Lett. **119**, 161101 (2017), arXiv:1710.05832 [gr-qc].

[9] E. Barausse, C. Palenzuela, M. Ponce, and L. Lehner, Phys. Rev. D **87**, 081506 (2013).

[10] J. Antoniadis, P. C. C. Freire, N. Wex, T. M. Tauris, R. S. Lynch, M. H. van Kerkwijk, M. Kramer, C. Bassa, V. S. Dhillon, T. Driebe, J. W. T. Hessels, V. M. Kaspi, V. I. Kondratiev, N. Langer, T. R. Marsh, M. A. McLaughlin, T. T. Pennucci, S. M. Ransom, I. H. Stairs, J. van Leeuwen, J. P. W. Verbiest, and D. G. Whelan, Science **340**, 448 (2013), arXiv:1304.6875 [astro-ph.HE].

[11] K. Lazaridis, N. Wex, A. Jessner, M. Kramer, B. W. Stappers, G. H. Janssen, G. Desvignes, M. B. Purver, I. Cognard, G. Theureau, A. G. Lyne, C. A. Jordan, and J. A. Zensus, Mon. Not. R. Astron. Soc. **400**, 805 (2009), arXiv:0908.0285 [astro-ph.GA].

[12] G. Desvignes, R. N. Caballero, L. Lentati, J. P. W. Verbiest, D. J. Champion, B. W. Stappers, G. H. Janssen, P. Lazarus, S. Osłowski, S. Babak, C. G. Bassa, P. Brem, M. Burgay, I. Cognard, J. R. Gair, E. Graikou, L. Guillemot, J. W. T. Hessels, A. Jessner, C. Jordan, R. Karuppusamy, M. Kramer, A. Lassus, K. Lazaridis, K. J. Lee, K. Liu, A. G. Lyne, J. McKee, C. M. F. Mingarelli, D. Perrodin, A. Petiteau, A. Possenti, M. B. Purver, P. A. Rosado, S. Sanidas, A. Sesana, G. Shaifullah, R. Smits, S. R. Taylor, G. Theureau, C. Tiburzi, R. van Haasteren, and A. Vecchio, Mon. Not. R. Astron. Soc. **458**, 3341 (2016), arXiv:1602.08511 [astro-ph.HE].

[13] J. Antoniadis, T. M. Tauris, F. Ozel, E. Barr, D. J. Champion, and P. C. C. Freire, arXiv e-prints , arXiv:1605.01665 (2016), arXiv:1605.01665 [astro-ph.HE].

[14] D. Mata Sánchez, A. G. Istrate, M. H. van Kerkwijk, R. P. Breton, and D. L. Kaplan, Mon. Not. R. Astron. Soc. **494**, 4031 (2020), arXiv:2004.02901 [astro-ph.HE].

[15] P. C. C. Freire, N. Wex, G. Esposito-Farèse, J. P. W. Verbiest, M. Bailes, B. A. Jacoby, M. Kramer, I. H. Stairs, J. Antoniadis, and G. H. Janssen, Mon. Not. R. Astron. Soc. **423**, 3328 (2012), arXiv:1205.1450 [astro-ph.GA].

[16] K. Liu, L. Guillemot, A. G. Istrate, L. Shao, T. M. Tauris, N. Wex, J. Antoniadis, A. Chalumeau, I. Cognard, G. Desvignes, P. C. C. Freire, M. S. Kehl, and G. Theureau, Mon. Not. R. Astron. Soc. **499**, 2276 (2020), arXiv:2009.12544 [astro-ph.HE].

[17] I. Cognard, P. C. C. Freire, L. Guillemot, G. Theureau, T. M. Tauris, N. Wex, E. Graikou, M. Kramer, B. Stappers, A. G. Lyne, C. Bassa, G. Desvignes, and P. Lazarus, Astrophys. J. **844**, 128 (2017), arXiv:1706.08060 [astro-ph.HE].

[18] J. M. Weisberg and Y. Huang, Astrophys. J. **829**, 55 (2016), arXiv:1606.02744 [astro-ph.HE].

[19] M. Kramer, I. H. Stairs, R. N. Manchester, M. A. McLaughlin, A. G. Lyne, R. D. Ferdman, M. Burgay, D. R. Lorimer, A. Possenti, N. D'Amico, J. M. Sarkissian, G. B. Hobbs, J. E. Reynolds, P. C. C. Freire, and F. Camilo, Science **314**, 97 (2006), arXiv:astro-ph/0609417 [astro-ph].

[20] A. D. Cameron, D. J. Champion, M. Kramer, M. Bailes, E. D. Barr, C. G. Bassa, S. Bhandari, N. D. R. Bhat, M. Burgay, S. Burke-Spolaor, R. P. Eatough, C. M. L. Flynn, P. C. C. Freire, A. Jameson, S. Johnston, R. Karuppusamy, M. J. Keith, L. Levin, D. R. Lorimer, A. G. Lyne, M. A. McLaughlin, C. Ng, E. Petroff, A. Possenti, A. Ridolfi, B. W. Stappers, W. van Straten, T. M. Tauris, C. Tiburzi, and N. Wex, Mon. Not. R. Astron. Soc. **475**, L57 (2018), arXiv:1711.07697 [astro-ph.HE].

[21] J. Zhao, L. Shao, Z. Cao, and B.-Q. Ma, Phys. Rev. D **100**, 064034 (2019).

[22] B. Bertotti, L. Iess, and P. Tortora, Nature **425**, 374 (2003).

[23] S. E. Field, C. R. Galley, J. S. Hesthaven, J. Kaye, and M. Tiglio, Physical Review X **4**, 031006 (2014), arXiv:1308.3565 [gr-qc].

[24] L. Shao, N. Sennett, A. Buonanno, M. Kramer, and N. Wex, Physical Review X **7**, 041025 (2017), arXiv:1704.07561 [gr-qc].